

# Oil Ganglia Mobility Enhancement by Droplet Formation for Surfactant Flooding in Porous Media

B. Haney<sup>1</sup> · T. Cochard<sup>1</sup> · A. Julien<sup>1</sup> · J. Wu<sup>1</sup> · R. Davis<sup>1</sup> · L. Xiao<sup>1,2</sup> · D. A. Weitz<sup>1,3,4</sup> · Y.-Q. Song<sup>1</sup>

Received: 2 August 2023 / Accepted: 14 December 2023 / Published online: 24 January 2024 © The Author(s), under exclusive licence to Springer Nature B.V. 2024

#### Abstract

We study the formation of oil droplets from an initially trapped large oil ganglion under surfactant flooding, using a microfluidic device consisting of a two-dimensional array of regularly spaced square posts. We observe that above a critical capillary number for oil mobilization, breakage of the ganglion results in the formation of either trapped patches spanning multiple pores or numerous mobile droplets that exit the device at a velocity comparable to the average flooding fluid velocity. These mobile droplets, however, are only observed when above a secondary capillary number threshold. The formation of these droplets is found to involve the simultaneous occurrence of three different passive droplet generation mechanisms where a droplet is formed as it is pulled by perpendicular fluid flow, as it is pulled by co-axial fluid flow, and or as it splits due to collision with a post. Our results show that oil breakthroughs only occur when the oil is in the form of mobile droplets, suggesting that droplet formation can be an important condition for the mobility of residual oil in porous media. Additionally, this post-array microfluidic device can be used for the production of monodisperse droplets whose size can be controlled by the spacing of the posts.

**Keywords** Porous media · Multiphase flow · Surfactant flow · Droplet formation

Wyss Institute for Biologically Inspired Engineering, Harvard University, Boston, MA, USA



B. Haney and T. Cochard have contributed equally.

D. A. Weitz weitz@seas.harvard.edu

Y.-Q. Song yqsong@g.harvard.edu

School of Engineering and Applied Sciences (SEAS), Harvard University, Cambridge, MA, USA

<sup>&</sup>lt;sup>2</sup> China University of Petroleum, Beijing, China

<sup>&</sup>lt;sup>3</sup> Department of Physics, Harvard University, Cambridge, MA, USA

# 1 Introduction

Multiphase flow in porous media under surfactant flooding is important for a diverse range of applications including oil and gas recovery and soil remediation. In these processes, one fluid phase exists as a stationary multi-pore connected region within a solid network until it is pushed by the flow of the second fluid (Iglauer et al. 2012; Datta et al. 2014; Oughanem et al. 2015; Wei, et al. 2020). Viscous forces, due to flow, must overcome the capillary forces, due to interfacial tension between the two phases, for mobilization and displacement of the trapped ganglion to occur, (Lake et al. 2014; Sheng 2011), yet this process is still not well understood. Several factors contribute to the complexity of ganglion displacement, including the intricate pore-scale geometry, multiphase interactions, and the presence of capillary forces. The interactions between the trapped oil ganglia and the displacing fluid, such as water or surfactant solutions, involve complex fluid–fluid and fluid–solid interactions that are challenging to characterize and predict accurately. Moreover, the heterogeneity of many porous systems and the variation in properties across different length scales further complicate understanding the mobilization and displacement processes.

Two-dimensional (2D) porous media are valuable models for studying and understanding the complex processes involved in the mobilization of trapped ganglia. The use of 2D porous media allows researchers to simplify and control experimental conditions, facilitating detailed investigations of fundamental mechanisms (Dias and Payatakes 1986a, 1986b). The interconnected pore network in 2D models captures essential aspects of fluid flow, transport, and displacement, providing insights into multiphase behavior during oil recovery processes (Lenormand 1999) Additionally, 2D models enable direct visualization of fluid—fluid and fluid—solid interactions, facilitating the observation and analysis of phenomena such as capillary trapping, wettability alteration, and displacement efficiency. While often used to study pore-scale phenomena by injecting a flooding fluid into porous media filled with continuous oil volume, the initial motion and displacement of small extended multi-pore ganglia under surfactant flooding have gained less attention (Yang et al. 2021). Understanding the onset and the modality of transport is an essential step to understanding the mobilization of oil ganglia in porous media.

In this contribution, we characterize the mobilization and subsequent droplet formation of an oil ganglion initially trapped among the columns in a geometrically controlled postarray device (PAD). We find that at low flow rates and low capillary numbers (Ca), the oil ganglion remains immobile. When Ca exceeds a critical value,  $Ca_c$ , the oil ganglion starts to move as the viscous force exceeds the capillary force, yet no oil is removed from the device. By further increasing the Ca, another threshold is reached which results in the formation of oil droplets that exit the device. Using a transparent PAD and fast camera, it is possible to analyze the threshold capillary number needed to produce droplets, which is required for oil removal. The oil droplets are formed from the edges of the ganglia due to several mechanisms: (Zhu and Wang 2017) crossflow droplet generation seen in T-junction geometries, co-flow generation seen in the co-axial alignment of flow channels, and breakup seen when an obstacle occupies a channel, all simultaneously occur in the PAD. These droplets are smaller than the size of the pore throat and flow past the posts so that they move near the average velocity of the flooding fluid. The existence of a threshold capillary number for droplet formation in surfactant flooding suggests that full mobilization and transport of the oil ganglion occurs only through free drop transport. These results provide insight into the mobilization of trapped oil via droplet formation in simple porous media geometries.



# 2 Methods

#### 2.1 Porous Media Fabrication

We use a 2D microfluidic model porous medium fabricated from micropatterned polydimethylsiloxane (PDMS) on a separate PDMS slab using 3D printing (Formlabs, Form3) to design the initial mold of the PAD, detailed in Fig. S1. The device's dimensions are  $80 \text{ mm} \times 30 \text{ mm} \times 0.5 \text{ mm}$ . Square posts of 1 mm are placed 0.5 mm apart from each other forming a continuous uniform array with a 1 mm pore size and 0.5 mm throat size, as shown in Fig. 1A.

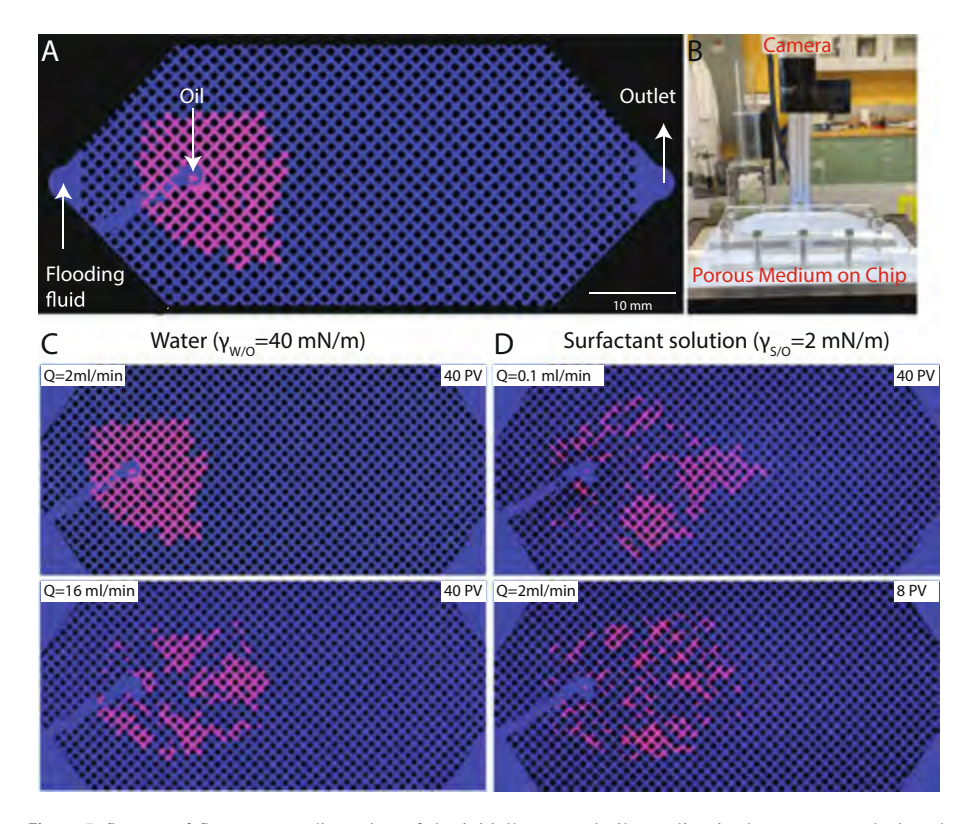


**Fig. 1** Influence of flow rate on disruption of the initially trapped oil ganglion in the post-array device. **A** The trapped oil ganglion before water or surfactant flooding where the oil, solid posts, and porous volume filled with the aqueous solution are labeled as red, black, and blue, respectively. **B** The camera is placed above the device to capture the automated injection and removal of the oil ganglion in experiments. **C** The top frame shows trapped oil ganglion after 40 PV using water as the flooding fluid at 2 ml/min, while the bottom frame shows the separation of the oil ganglion into a few discrete ganglia after 40 PV using water as the flooding fluid at 16 ml/min. **D** The top frame shows the separation of the oil ganglion into several discrete ganglia of various sizes after 40 PV using surfactant solution as the flooding fluid at 0.1 ml/min, while the bottom frame shows the separation of the oil ganglion into several small discrete ganglia along with the formation of freely moving droplets that exit the device after 8 PV using surfactant solution as the flooding fluid at 2 ml/min



# 2.2 Automized Acquisition and Fluid Injection

Three syringe pumps containing, respectively, isopropanol for cleaning the device between experiments, oil, and flooding fluid (water or surfactant solutions) are controlled by a Python computer program as shown in Fig. S2. A typical experiment consists of six steps: (1) cleaning the PAD with the isopropanol solution with pump P2, (2) Imbibing the PAD with the flooding solution with pump P1, (3) taking a snapshot, (4) injecting slowly the residual oil into the device by opening the valve on the oil line, (5) closing the valve, and (6) injecting the flooding solution at a flow rate Q while the camera is recording at a frame rate corresponding to Q(ml/min) \* 10. This experiment is then repeated multiple times by varying the injection flow rate for each flooding fluid as shown in Fig. S3.

## 2.3 Fluids, Interfacial Tension, and Surface Tension

The oil used in this study is a mineral oil (CAS 8042–47-5) with a density of 0.84 g/cm3, viscosity  $\mu_{oil} = 10cP$  at 25 °C. For the water injection, we use deionized water mixed with a blue dye, methylene blue (CAS 122965–43-9) giving us a great contrast between the two phases. The surfactant solution is a mixture of deionized water mixed with 1 g/l sodium dodecylbenzene sulfonate (SDBS, C18H29NaO3S, CAS 25155–30-0), 5 g/l sodium chloride (NaCl, CAS 7647–14-5), and a blue dye (Wright stain, CAS 68988–92-1). The viscosity of the two flooding solutions is similar,  $\mu_S = 1cP$  at 25 °C.

Interfacial properties characterization between the two phases and PDMS was conducted. The addition of methylene blue did not show a noticeable difference in interfacial tension measurements; therefore, all measurements were recorded with the dye in solutions. Pendant drop tests show that the interfacial tension between the oil phase and water is  $\sigma_{wo} = 40mN/m$ , while the interfacial tension between the oil phase and the surfactant solution is  $\sigma_{so} = 2mN/m$ . The use of the surfactant solution, therefore, led to an 8 times lower interfacial tension as shown in Fig. S4A. The contact angle between the oil and water with PDMS is approximately  $\theta = 140^{\circ}$ , as shown in Fig. S4B.

# 3 Results and Discussion

## 3.1 Experimental Approach

The PAD is initially filled with the aqueous flooding fluid and then held under a vacuum to remove any air. There is no PAD surface treatment. A calibrated volume of oil,  $V_0 = 60\mu l$  (10% of the total pore volume), is inserted to sit at the inlet of the device indicated by the arrows in Fig. 1A. All fluids exit the PAD through the same outlet. To enable visualization of the flow of oil and water phases, a camera is placed above the device, as shown in Fig. 1B. For each experiment, the frame rate is chosen to be proportional to the flow rate of the injected fluid, Q. In the images, we label the oil, solid posts, and porous volume filled with the aqueous solution in red, black, and blue, respectively, as shown in Fig. 1. We compare the effects of interfacial tension between the oil and water on oil mobilization by flooding with either deionized water,  $W_f$ , or a surfactant and salt in water solution,  $S_f$ . The viscosity and density of these two flooding fluids are relatively similar due to the small



amount of salt and surfactant added. The ganglion movement and progression are characterized as a function of the injected flooding fluid volume normalized by the total pore volume of the PAD, PV.

For  $W_f$  flood at low flow rates, the initial oil ganglion shows no sign of movement, as seen in Fig. 1C. A  $W_f$  flowrate of 16 ml/min causes viscous fingering of the oil ganglion leading to the formation of multiple discrete ganglia trapped in the pores of the PAD at 40 PV. Despite the higher  $W_f$  flow rate, no oil exits the PAD. When using the  $S_f$  to decrease the interfacial tension, much lower flowrates mobilize the oil as seen in Fig. 1D. At a flow rate of 0.1 ml/min, the initial oil ganglion breaks into multiple discrete ganglia with an even more pronounced occurrence of viscous fingering. However, after 40 PV is injected, all the oil still remains fully trapped in the PAD. By contrast, flow rates above 0.1 ml/min yield drastic changes. At 2 ml/min, not only do discrete ganglia become smaller and more numerous, but large droplets start forming after injection of 8 PV whereupon they continue downstream as free drops as shown in Fig. 1D (bottom). In all cases, oil only exits the device when free drops are formed.

We observed that the free drop formation and subsequent oil removal are the results of several distinct breakup events after the ganglion is mobilized in the PAD. First, the viscous force pushing the oil ganglia downstream overcomes the capillary forces holding them in place thereby initializing downstream motion. This leads to a combination of events that result in either trapping the oil or in the formation of free drops that can then exit the PAD. After the initial oil mobilization, the flooding fluid can penetrate the oil volume via viscous fingering to produce smaller size ganglia. These ganglia either remain trapped or break into intermediate-size droplets which can then be further broken into much smaller free drops that ultimately leave the device. When using  $W_{f}$ , the oil breakage process stops at the formation of the intermediate droplets that remain trapped in the device. However, decreasing the interfacial tension using the  $S_f$  flooding fluid can lead to a variety of outcomes that include free drop formation after viscous fingering, free drop formation after the breakage of intermediate droplets, or even free drop formation from the edges of the ganglia immediately after initial mobilization as seen in video S1. Oil removal from the PAD only occurs upon the formation of these free drops which is made possible by the low interfacial tension. The ganglion breakage process responsible for the free drops is governed by a balance between viscous and capillary forces.

#### 3.2 Oil Mobilization

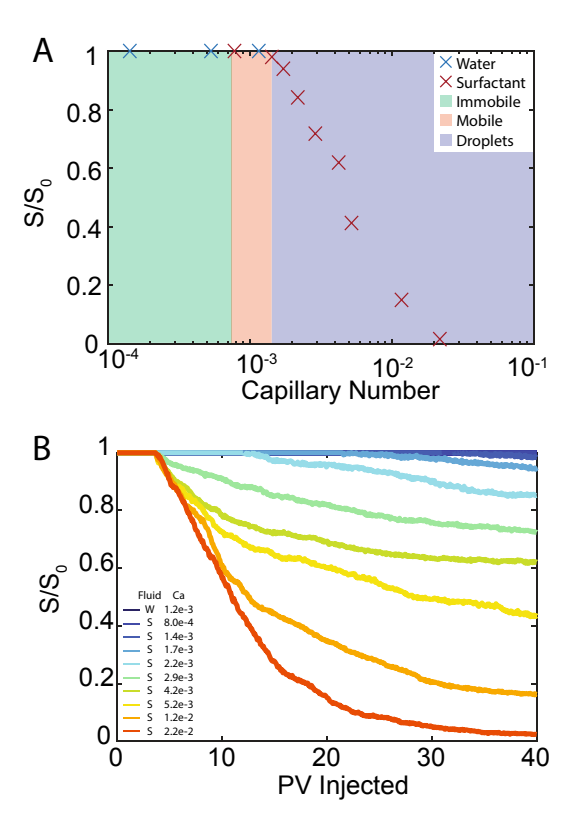
Initial oil ganglion movement requires overcoming the capillary forces trapping it in the pores of the PAD. The ratio of viscous forces to capillary forces is conventionally used to predict multiphase flow behavior, (Guo 2017; Hirasakl 1991; Rucker et al. 2015) and is expressed in porous media (Melrose and Brandner 1974) as the microscopic capillary number, (Foster 1973; Guo et al. 2022)  $Ca = \frac{\mu U_f}{\sigma \phi}$ , where  $\mu$  is the flooding fluid viscosity,  $\frac{U_f}{\phi}$  is the average velocity of the flooding fluid,  $\phi$  is the porosity of the media equal to 0.5, and  $\sigma$  is the interfacial tension between the oil and flooding fluid.

Upon initial mobilization of the oil ganglion, capillary number-dependent displacement and eventual droplet formation may occur. Using water flooding, either the initial ganglion never moves, or it is mobilized and separated into ganglia at a certain Ca, yet droplets are never formed.  $W_f$  flows against the oil ganglia where we see no discernable movement of the oil to the next pore. At a capillary number of  $1.1x10^{-4}$ , the capillary forces dominate



viscous forces, and the oil ganglion remains motionless and trapped within the posts. When the flow rate is increased to yield  $Ca = 1.2 \times 10^{-3}$ , the oil ganglion is mobilized temporarily and separated into several large discrete ganglia, but no droplets are formed, and oil never exits the PAD. Oil saturation as a function of capillary number is shown in Fig. 2A where saturation is represented by the ratio of final oil saturation, S, to initial oil saturation,  $S_0$ . The blue markers on the plot represent the flooding fluid  $W_f$  where we see oil saturation remains unaffected by the decade change in capillary number. The shaded regions on the plot show the point of oil mobilization and the point when droplet formation is expected. Although  $W_f$  mobilizes the oil ganglia, saturation remains high because no droplets form at the low capillary numbers. With  $S_{t}$  mobilization and droplet formation are achieved due to the lower flow rates permitting higher capillary numbers in the PAD. When flooding fluid  $S_f$  flows against the oil ganglion at  $Ca = 8x10^{-4}$  oil is mobilized, yet no droplets are formed, and oil never exits the PAD. At  $Ca = 1.4x10^{-3}$  we see that the oil is mobilized, and droplets are eroded from the ganglia edges and flow downstream to exit the chip. As the capillary number is increased, more oil can exit the PAD. These data show that there is a critical capillary number in the range of  $5.5x10^{-4}$  to  $8x10^{-4}$  needed to temporarily mobilize the initially trapped oil ganglion. Without surfactant, increasing the Ca leads to an increase in the number of discrete ganglia and viscous fingering yet eventual oil trapping occurs with no droplet formation and no oil removal from the PAD. Adding surfactant to the flooding fluid causes a Ca-dependent oil saturation where at low Ca, oil is mobilized with no droplet formation, yet as Ca is increased to a threshold value, droplets form, and

Fig. 2 Capillary desaturation curve and oil saturation in the PAD. A The oil saturation as a function of capillary number where three separate zones indicate immobilization, mobilization, and formation of freely moving droplets. The blue and red "X" represent PAD flooding with pure water or a surfactant solution, respectively. B The oil saturation as a function of pore volume for different capillary numbers





oil exits the PAD. Oil saturation as a function of pore volume injected seen in Fig. 2B shows a nearly 100% decrease in the amount of oil left in the device over a Ca range spanning 2 orders of magnitude. At lower Ca, discrete ganglia are formed after initial breakage and remain trapped. At this Ca, droplets are not observed to erode from the oil ganglia edges. This limitation becomes more pronounced as the Ca is decreased and may be due to lower local flow velocities gradient around the immobilized oil.

The observation of oil removal via formation of droplets suggests a mechanism of twophase transport via smaller-than-pore-size droplets and an associated threshold Ca. A similar scenario for mobility has previously been discussed for oil ganglia breakage in the coflow of two immiscible fluids in a porous medium but the presence of droplets was not mentioned (Datta et al. 2014). With the addition of surfactant in the flooding fluid, both the critical and threshold Ca numbers are decreased, and we get the formation of the free droplets necessary to achieve oil removal. Although these are the results for the considered surface wetting properties of the material and fluids in this study, changes in wettability may influence droplet formation mechanisms. This study has also been conducted with random porous geometries where the same behavior is observed in video S2, indicating that our observations may be applicable to other pore geometries.

# 3.3 Droplet Formation

Oil removal in the PAD is due to the formation of mobile oil droplets eroded from the edges of the ganglia in a series of separate fluid mechanics commonly observed in microfluidic droplet-generating devices (Zhu and Wang 2017). The oil displacement is achieved via initial movement of the full oil body, viscous fingering, and intermediate or free drops formation. Free drop formation can be described by three different dynamics: crossflow of fluids, co-flow of fluids, and breakup. Upon mobilization of the full oil body, oil droplets are eroded from the ganglia via crossflow when a portion of the oil protrudes into the flooding fluid volume perpendicular to its flow direction. If the formed droplet is larger than one pore size or many droplets coalesce into one, it may either flow between PAD structures pulled by the flooding fluid in co-flow or collide with the structures to separate into two individual droplets in the breakup. These three different steps can occur after the initial oil body movement and lead to an eventual oil breakthrough. As the oil is completely broken up at later PV, the free drops have exited the device while large discrete ganglia remain trapped where no more droplets can form as seen in the video S1.

### 3.3.1 Crossflow

Oil ganglia motion and subsequent free drop formation are the cause of oil removal from the PAD. After the ganglion is pushed forward as a whole, flooding fluid penetrates the volume and oil slowly moves outward. As fluid flows around the edges of the mobilized oil ganglia, droplets form due to crossflow mechanics commonly characterized in T-junction droplet microfluidics (Zagnoni et al. 2010) Crossflow droplet formation in this PAD occurs similarly to the squeezing drop formation in traditional T-junction fluid flow where free drops are produced when the edges of the oil ganglia push into the flooding fluid stream as depicted in Fig. 3A. In the porous media device, the droplet fills the space between two posts and slowly pushes toward the open pore where flooding fluid is flowing in the perpendicular direction. The oil protrusion occupies a large enough percentage of the pore space to obstruct the fluid flow causing a pressure gradient across the attached oil droplet.



## A Crossflow

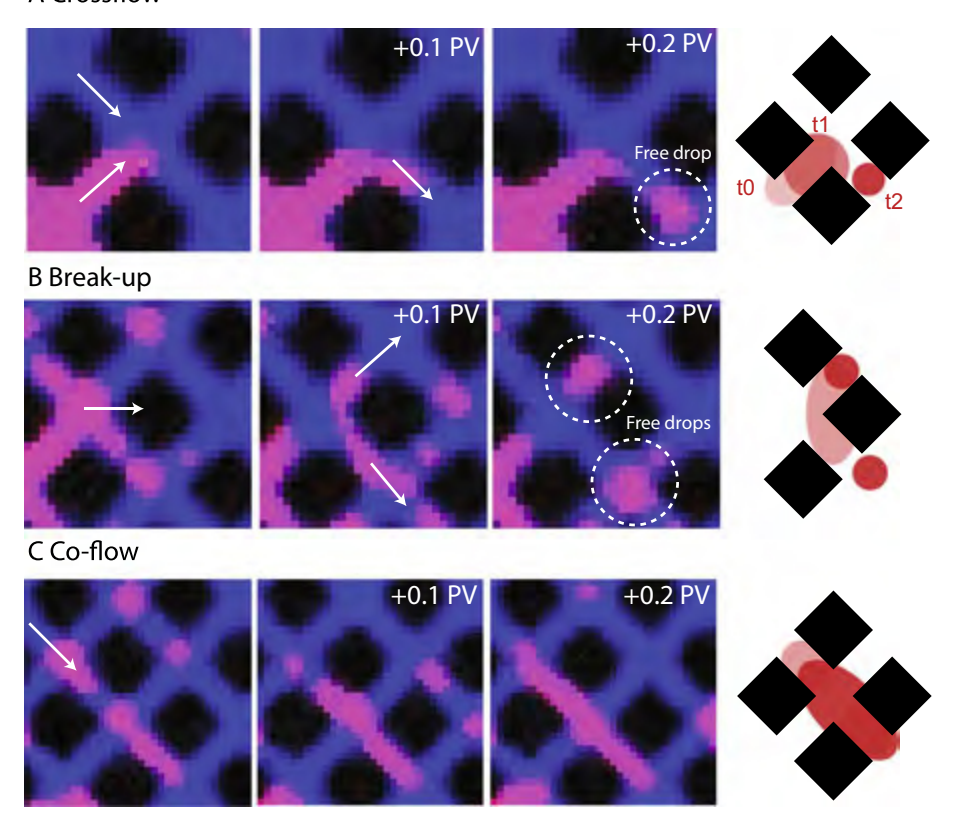


**Fig. 3** Droplet formation mechanisms in the post-array device. **A** The oil is pushed between two posts where the perpendicular flow of the flooding fluid shears and breaks a droplet from the oil surface. **B** The oil is pushed and collides with the edge of a post where it splits into two separate freely moving droplets. **C** Oil is pulled downstream by the concentric flow of the flooding fluid until a droplet is formed that can merge with droplets further downstream. The oil, solids posts, and flooding fluids are colored red, black, and blue, respectively

The pressure difference upstream and downstream of the drop eventually overcomes the Laplace pressure within the drop tip and deforms. The neck thins, and the droplet breaks away to flow downstream between the posts. The squeezing regime is characterized by low capillary numbers of less than order  $10^{-2}$ . In this regime, droplet size can be approximated by the channel size when the dispersed phase fluid flow rate is much lower than the continuous phase (Menech et al. 2008). In the PAD experiments, the oil is mobilized solely by the flooding fluid; therefore, for high continuous phase flowrate and low dispersed phase flowrate, one can expect droplets to be the approximate size of the channel. Our results indeed show droplets very close to pore size at the low  $10^{-4}$  capillary numbers indicative of squeezing T-junction droplet formation.



## 3.3.2 Breakup

The formation of free drops due to breakup when an oil volume collides with a post in the PAD can be seen in Fig. 3B. Breakup refers to the collision of a larger-than-channel size droplet with an obstacle and the subsequent formation of two daughter droplets of smaller size. It is characterized by the formation of two menisci that fill the gaps on the sides of the obstacle and progress at different speeds to create different size droplets (Protiere et al. 2010) At higher dispersed phase capillary numbers, as viscous forces become more relevant, the two menisci travel around the obstacle at nearly the same speed, resulting in less variance between the sizes of the daughter droplets. In breakup experienced in the PAD, a separated and discrete portion of oil ganglia traveling near the flooding fluid velocity collides with the edge of a post. Two menisci form around the post and split into separate droplets of nearly the same size and continue to flow downstream as seen in Fig. 3B. Droplet formation due to breakup leads to two new droplets of similar size that will either traverse the length of the PAD as free drops or coalesce and exit the device due to co-flow.

## 3.3.3 Co-flow

Co-flow mechanics also occur after the initial oil ganglia mobilization. In the PAD, flooding fluid initiates mobility of the oil ganglia eventually penetrating the volume and eroding droplets from the edges. Surfactant solution that has invaded the oil ganglia area starts to push the oil between two posts where a meniscus is formed. When the viscous drag of the flooding fluid flowing across the oil meniscus becomes comparable to the surface tension, an oil lobe of channel width extends further downstream between posts. Droplet breakoff occurs as a small undulation happens along its extension resulting in the separation of channel-width oil ganglia that can span the length of two posts as seen in Fig. 3C. The droplet formation is reminiscent of that seen in co-flow single-channel droplet makers in the dripping regime where droplet formation is characterized by the dispersed phase Weber number, the balance of droplet inertial forces with surface tension, and continuous phase capillary number, the balance of viscous stress with surface tension (Utada et al. 2007) Assuming the co-flow oil in the PAD achieves a velocity close to the flooding fluid upon break-off, the oil Weber and flooding fluid capillary numbers are  $2 \times 10^{-3}$  and  $9 \times 10^{-4}$ , respectively. At a dispersed to continuous viscosity ratio of 10, our results clearly show droplet formation in the dripping regime (Utada et al. 2007) where droplet size is set by the "tip", or orifice diameter. In this work co-flow results in the flooding fluid flowing in the same direction of the broken-off oil ganglia carrying it to the end of the PAD. This discrete oil volume can traverse the full length of the device until breakthrough, collide with a post for breakup, or coalesce and repeat the cycle until the dispersed phase is trapped and no droplets can form.

## 3.4 Free Drops

The formation of free drops results in the fast breakthrough of the oil ganglia and subsequently formation of monodispersed droplets. This is ideal for the throughput enhancement of emulsifier devices. The number, size, and speed of droplets are characterized based on analyzing a specific area on the PDMS chip as shown in Fig. 4. To quantify these parameters, we focus on a region toward the outlet shown by the red rectangle in Fig. 4A. As droplets pass through this analysis area, particle tracking software



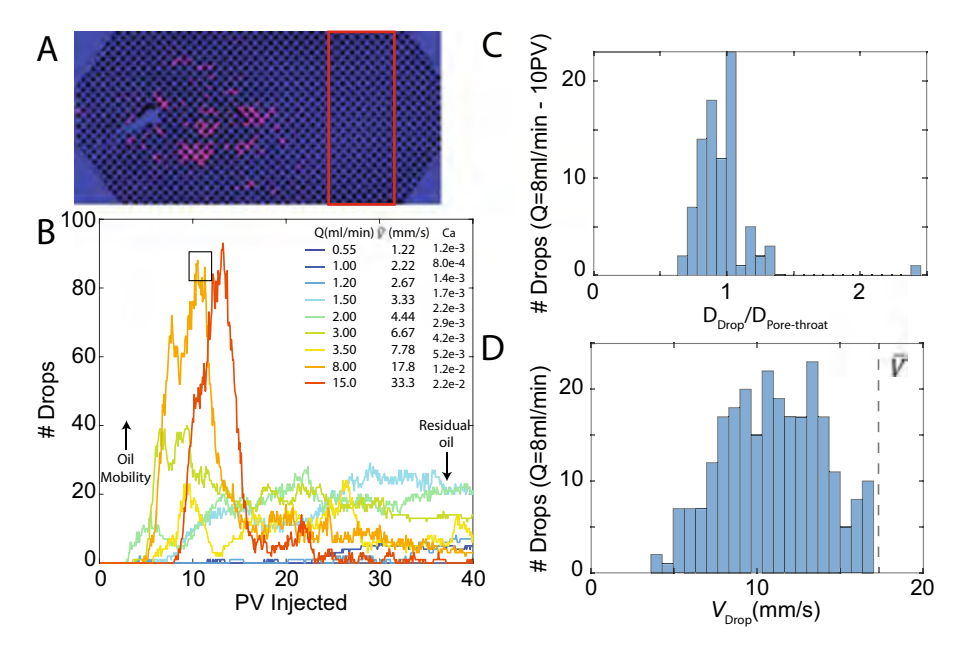


**Fig. 4** Droplet Quality in the post-array device. **A** The red box indicates the area used to characterize droplets exiting the device. **B** The number of droplets as a function of pore volume for different capillary numbers. **C** The droplet size distribution showing near pore-size droplets at 10 PV using surfactant flooding fluid at 8 ml/min. **D** The average velocity of freely moving droplets using surfactant flooding fluid at 8 ml/min where the dotted line represents the average velocity of the flooding fluid in the device

(TrackMate plugin on ImageJ) collects data to characterize free drops formed as PV increases. At low flow rates, there is no movement of the oil ganglia until 25 PV is injected where we found at least 5 drops per pore volume injected consistently exiting the PAD up to 40 PV as shown by the blue lines in Fig. 4B. As the flow rate is increased up to 2 ml/min, the number of droplets increases and there are at least 20 drops per PV injected consistently exiting the porous media device from 20 to 40 PV. At higher flow rates, resulting in a concomitant capillary number increase, most of the droplet formation happens faster, after less than 20 PV are injected. In this case, droplet movement is no longer consistent over a range of PV, but instead, much of the oil ganglia volume is broken into droplets and exits the device near 1 PV. At the highest injection flow rates, there is a peak in the number of drops around 10 PV followed by a dramatic decrease as oil exits the device. Overall, oil mobility and residual oil saturation increase and decrease, respectively, as the capillary number increases as shown in Fig. 4B.

The droplets formed in our PAD are found to exhibit a narrow size distribution. The droplet size distribution after 10 PV of surfactant solution at Q = 8ml/min shows that most of the droplets are at the size of the pore throat or slightly smaller, as seen in Fig. 4C. This shows great control of the final droplet size with the PAD making it a great candidate for enhanced throughput emulsion production. Indeed, droplets formed in the porous media device travel fast at capillary numbers of  $10^{-3}$ . As a result of their size that is comparable to the pore throat size, the oil droplets can travel almost as fast as the continuous phase fluid as seen in Fig. 4D.



Surfactant solution permits deformation of the oil–water interface allowing the formation and mobility of pore throat size droplets at lower flow rates. This can be useful for droplet-making devices that strive to increase throughput without droplet buildup at the exit that causes increased polydispersity (Stolovicki et al. 2018). We can see that using the surfactant solution flooding fluid at  $Ca = 2.2 \times 10^{-2}$  (15 ml/min), approximately 98% of the initial oil ganglia has exited after injecting nearly 35 PV, as shown in Fig. 2A. It is equivalent to 84 s to remove the full amount of oil equating to a droplet throughput of 2.5 ml/hr on a single PDMS chip. This is double what is commonly achieved on a single-channel PDMS microfluidic chip for making droplets slightly smaller than 1 mm and, comparable to the 3 ml/hr droplet throughput achieved using a micropillar array single-channel microfluidic device (Akbari et al. 2017).

## 4 Conclusion

We use a transparent post-array device with controllable pore and post architecture to observe the basic processes occurring in multiphase flow. Oil displacement has been characterized by various fundamental mechanisms where after the initial movement of the full oil body, a threshold capillary number must be reached to trigger subsequent passive droplet generation mechanisms to form many free drops that flow and exit the PAD at high flooding fluid velocities. Droplets form from a ganglion due to simultaneous co-flow, crossflow, and breakup by fluid flooding which has not been given much attention in multiphase flow in porous media studies. The current work does not predict what would happen in conditions of varying wettability or porosity; therefore, future experiments using wettable synthetic materials and rock samples will further improve our understanding of capillary number-dependent droplet formation's relevance where oil is recovered in porous media.

While this work focuses on the fundamental oil transport mechanisms in a structured array microfluidic chip, the potential application in uniform emulsion droplet formation is most apparent. At relatively low flooding fluid flow rates, the PAD can be used to efficiently create uniform-size droplets using a constant pore throat size, and/or interfacial tension between the liquids. The PAD may have the potential to mitigate droplet build-up at the exit, limiting the increase in polydispersity experienced in some other high-throughput microfluidic devices. The presence of columns throughout the PAD also makes it more robust than single-channel devices as the latter can be easily clogged by debris and dust trapped in the flow paths. This can be applied to the production and control of uniform emulsion droplets in diverse applications such as energy storage (Amit et al. 2021) and drug delivery studies with microfluidics (Dong, et al. 2018). Furthermore, these results can be valuable to soil remediation and enhanced oil recovery in highlighting the role of interfacial tension and the unseen oil removal mechanics. Many studies in oil recovery show disconnected residual oil ganglia much larger than the pore size after a water flood (Iglauer et al. 2012; Oughanem et al. 2015; Krummel et al. 2013). Our results show that it may be possible to increase oil removal by focusing on free-droplet generation as a novel mechanism for oil removal and recovery. In other transparent porous media experiments where the onset of droplet formation can be assessed, we expect that the droplet speed, size, and quantity can be compared using the nondimensional quantity or ratio of droplet size to the smallest length scale, making our findings applicable to other systems. It would be interesting to explore droplet formation in 3D porous media (Sheng 2011) to evaluate the potential oil droplet formation and enhanced oil sweeping efficiency.



**Supplementary Information** The online version contains supplementary material available at https://doi.org/10.1007/s11242-023-02050-z.

**Acknowledgements** This research was supported by Chinese University of Petroleum Beijing through the Harvard-CUPB joint laboratory on Petroleum Science and the Harvard MRSEC (NSF, DMR-2011754). We thank Profs. J. Bibette and H. A. Stone for insightful discussions.

## **Declarations**

**Conflicts of interest** There are no conflicts to declare.

## References

- Akbari, S., Pirbodaghi, T., Kamm, R.D., Hammond, P.T.: A versatile microfluidic device for high throughput production of microparticles and cell microencapsulation. Lab Chip 17, 2067–2075 (2017). https://doi.org/10.1039/c6lc01568a
- Amit, L., Naar, D., Gloukhovski, R., la O, G.J., Suss, M.E.: A single-flow battery with multiphase flow. Chemsuschem 14, 1068–1073 (2021). https://doi.org/10.1002/cssc.202002135
- Datta, S.S., Dupin, J.B., Weitz, D.A.: Fluid breakup during simultaneous two-phase flow through a threedimensional porous medium. Phys. Fluids (2014). https://doi.org/10.1063/1.4884955
- De Menech, M., Garstecki, P., Jousse, F., Stone, H.A.: Transition from squeezing to dripping in a microfluidic T-shaped junction. J. Fluid Mech. **595**, 141–161 (2008). https://doi.org/10.1017/s002211200700910x
- Dias, M.M., Payatakes, A.C.: Network models for 2-phase flow in porous-media 2. Motion of oil ganglia. J. Fluid Mech. **164**, 337–358 (1986a). https://doi.org/10.1017/s0022112086002586
- Dias, M.M., Payatakes, A.C.: Network models for 2-phase flow in porous-media 1. Immiscible microdisplacement of nonwetting fluids. J. Fluid Mech. 164, 305–336 (1986b). https://doi.org/10.1017/s0022 112086002574
- Dong, L., et al.: Integrated microfluidic device for drug studies of early C elegans embryogenesis. Adv. Sci. (2018). https://doi.org/10.1002/advs.201700751
- Foster, W.R.: A low-tension waterflooding process. J. Petrol. Technol. 25, 205–210 (1973). https://doi.org/10.2118/3803-pa
- Guo, H., et al.: Proper use of capillary number in chemical flooding. J. Chem. (2017). https://doi.org/10. 1155/2017/4307368
- Guo, H., Song, K., Hilfer, R.: A brief review of capillary number and its use in capillary desaturation curves. Transp. Porous Media 144, 3–31 (2022). https://doi.org/10.1007/s11242-021-01743-7
- Hirasakl, G.J.: Wettability: fundamentals and surface forces. SPE Form. Eval.eval. 6, 217–226 (1991). https://doi.org/10.2118/17367-pa
- Iglauer, S., Ferno, M.A., Shearing, P., Blunt, M.J.: Comparison of residual oil cluster size distribution, morphology and saturation in oil-wet and water-wet sandstone. J. Colloid Interface Sci. 375, 187–192 (2012). https://doi.org/10.1016/j.jcis.2012.02.025
- Krummel, A.T., Datta, S.S., Munster, S., Weitz, D.A.: Visualizing multiphase flow and trapped fluid configurations in a model three-dimensional porous medium. AIChE J. J. 59, 1022–1029 (2013). https://doi.org/10.1002/aic.14005
- Lake, L., Johns, R. T., Rossen, W. R. & Pope, G. A. In: Fundamentals of Enhanced Oil Recovery, Society of Petroleum Engineers, (2014)
- Lenormand, R. In: Po-zen Wong (ed.) Experimental Methods in the Physical Sciences vol. 35, pp. 43–68. Academic Press, Cambridge (1999)
- Melrose, J.C., Brandner, C.F.: Role of capillary forces in determining microscopic displacement efficiency for oil-recovery by waterflooding. J. Can. Pet. Technol. 13, 54–62 (1974). https://doi.org/10.2118/74-04-05
- Oughanem, R., et al.: A multi-scale investigation of pore structure impact on the mobilization of trapped oil by surfactant injection. Transp. Porous Media 109, 673–692 (2015). https://doi.org/10.1007/s11242-015-0542-5
- Protiere, S., Bazant, M.Z., Weitz, D.A., Stone, H.A.: Droplet breakup in flow past an obstacle: a capillary instability due to permeability variations. Europhys. Lett.. Lett. (2010). https://doi.org/10.1209/0295-5075/92/54002



- Rucker, M., et al.: From connected pathway flow to ganglion dynamics. Geophys. Res. Lett. Res. Lett. 42, 3888–3894 (2015). https://doi.org/10.1002/2015gl064007
- Sheng, J. J. In: James J. Sheng (ed.) Modern Chemical Enhanced Oil Recovery, pp. 239–335. Gulf Professional Publishing, Houston, (2011)
- Stolovicki, E., Ziblat, R., Weitz, D.A.: Throughput enhancement of parallel step emulsifier devices by shear-free and efficient nozzle clearance. Lab Chip 18, 132–138 (2018), https://doi.org/10.1039/c7lc01037k
- Utada, A.S., Fernandez-Nieves, A., Stone, H.A., Weitz, D.A.: Dripping to jetting transitions in coflowing liquid streams. Phys. Rev. Lett. (2007). https://doi.org/10.1103/PhysRevLett.99.094502
- Wei, B., et al.: Nuclear magnetic resonance (NMR) mapping of remaining oil distribution during sequential rate waterflooding processes for improving oil recovery. J. Pet. Sci. Eng. (2020). https://doi.org/10. 1016/j.petrol.2020.107102
- Yang, W., Lu, J., Wei, B., Yu, H., Liang, T.: Micromodel studies of surfactant flooding for enhanced oil recovery: a review. ACS Omega 6, 6064–6069 (2021). https://doi.org/10.1021/acsomega.0c05750
- Zagnoni, M., Anderson, J., Cooper, J.M.: Hysteresis in multiphase microfluidics at a T-junction. Langmuir **26**, 9416–9422 (2010). https://doi.org/10.1021/la1004243
- Zhu, P.A., Wang, L.Q.: Passive and active droplet generation with microfluidics: a review. Lab Chip 17, 34–75 (2017). https://doi.org/10.1039/c6lc01018k

**Publisher's Note** Springer Nature remains neutral with regard to jurisdictional claims in published maps and institutional affiliations.

Springer Nature or its licensor (e.g. a society or other partner) holds exclusive rights to this article under a publishing agreement with the author(s) or other rightsholder(s); author self-archiving of the accepted manuscript version of this article is solely governed by the terms of such publishing agreement and applicable law.

